Future Dual-Frequency GPS Navigation System for Intelligent Air Transportation Under Strong Ionospheric Scintillation

Jiwon Seo, *Member, IEEE*, and Todd Walter

***Abstract*—GPS technology is essential for future intelligent air transportation systems such as the Next Generation Air Transportation System (NextGen) of the United States. However, observed deep and frequent amplitude fading of GPS signals due to ionospheric scintillation can be a major concern in expanding GPS-guided aviation to the equatorial area where strong scintillation is expected. Current civil GPS airborne avionics track signals at a single frequency (L1 frequency) alone because it was the only civil signal available in the frequency band for aviation applications. The first GPS Block IIF satellite was launched in May 2010. This next-generation satellite transmits a new civil signal at the L5 frequency, which can be used for air transportation. This paper investigates a possible improvement in the availability of GPS-based aircraft landing guidance down to 200 ft above the runway, which is also known as Localizer Performance with Vertical Guidance (LPV) 200, under strong ionospheric scintillation when dual-frequency signals are available. Based on the availability study, this paper proposes and justifies a GPS aviation receiver performance standard mandating fast reacquisition after a very brief signal outage due to scintillation. In order to support a temporary single-frequency operation under a single-frequency loss due to scintillation, a new vertical protection level (VPL) equation is proposed and justified. With this new performance requirement and new VPL equation in place, 99% availability of LPV-200 would be attainable, rather than 50% at the current standards, even under the severe scintillation scenarios considered in this paper.**

***Index Terms*—Availability, dual-frequency global positioning system (GPS) aviation, intelligent air transportation, ionospheric scintillation.**

I. Introduction

THE GPS [1]–[3] is an essential technology for future intelligent air transportation systems [4]–[6] such as the Next Generation Air Transportation System (NextGen) of the United States [7], [8]. The first GPS Block IIF satellite was successfully launched in May 2010 [9], [10] and was a major step in GPS aviation because this next-generation satellite transmits a new civil signal at the L5 frequency (1176.45 MHz). Unlike the L2 frequency (1227.6 MHz), L1 (1575.42 MHz) and L5 frequencies are within the Aeronautical Radio Navigation Service band and are usable for aviation applications.

Together with the civil signal at the L1 frequency, this new civil signal at L5 enables eliminating ionospheric delay error up to the first order [11], [12]. Hence, future dual-frequency airborne GPS avionics tracking L1 and L5 civil signals can directly resolve the ionospheric delay, which is the biggest error source for the current single-frequency GPS aviation. In addition to this well-known benefit, the new L5 signal can improve the availability of GPS-based aircraft landing guidance service during strong ionospheric scintillation.

Electron density irregularities in the ionosphere can cause constructive and destructive interference of transionospheric radio waves. As a result, a receiver experiences deep (more than 25 dB) and frequent signal fades, as shown in Fig. 1 (bottom). This phenomenon is known as ionospheric scintillation [13]–[17]; its effects on Global Navigation Satellite Systems (GNSS) such as GPS in the United States are summarized in [18] and [19]. Humphreys *et al.* [20]–[22] analyzed scintillation effects on GPS receivers. In order to characterize GPS signal fades under strong scintillation in the short timescale of a receiver tracking loop closure, a limited number of high-rate (20 or 50 Hz) GPS data sets from the past solar maximum were analyzed in [23] and [24].

Specific to aviation applications, Conker *et al.* [25] simulated the global trend of aviation availability based on a wideband ionospheric scintillation model [26]. Akala *et al.* [27] examined the potential impacts of strong scintillation on equatorial aviation applications. Seo *et al.* [28] introduced a carrier smoothing filter model of an aviation receiver and analyzed the operational availability of vertical and horizontal navigation at a single equatorial location during an observed strong scintillation period from the past solar maximum. The low satellite-to-satellite correlation of signal fades observed during the past solar maximum [29] indicates a significant availability benefit from the geometric diversity of GNSS satellites.

Future dual-frequency GPS avionics will track L1 and L5 signals simultaneously; therefore, there is a backup frequency available when the avionics briefly lose one frequency due to scintillation. Thus, this frequency diversity of GPS signals is expected to increase the operational availability of GPS aviation under scintillation, although a qualitative analysis has not been previously performed. Considering the practical importance of

Manuscript received July 22, 2013; revised December 21, 2013 and March 7, 2014; accepted March 7, 2014. Date of publication April 9, 2014; date of current version September 26, 2014. This work was supported in part by the Federal Aviation Administration under Grant CRDA 08-G-007 and in part by the Korean Ministry of Science, ICT, and Future Planning through the IT Consilience Creative Program supervised by the National IT Industry Promotion Agency under Grant NIPA-2014-H0201-14-1002. The Associate Editor for this paper was J.-P. B. Clarke.

J. Seo is with the School of Integrated Technology and the Yonsei Institute of Convergence Technology, Yonsei University, Incheon 406-840, Korea (e-mail: jiwon.seo@yonsei.ac.kr).

T. Walter is with the Department of Aeronautics and Astronautics, Stanford University, Stanford, CA 94305-4035 USA.

Color versions of one or more of the figures in this paper are available online at http://ieeexplore.ieee.org.

Digital Object Identifier 10.1109/TITS.2014.2311590

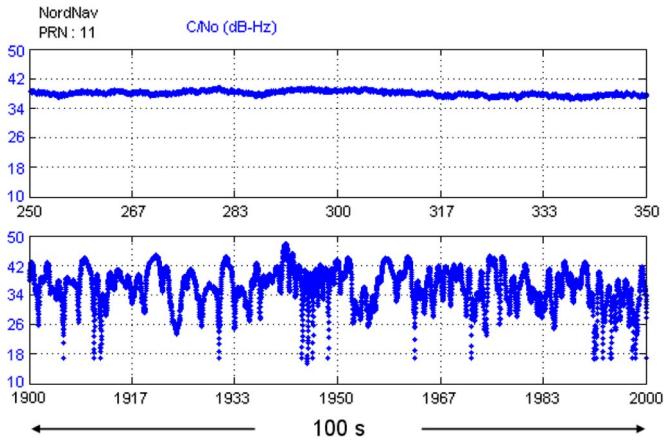

Fig. 1. (Bottom) Signal-to-noise-density ratio (C/N_0) fluctuations under strong ionospheric scintillation. (Top) Under a nominal condition without scintillation, C/N_0 remains almost constant. This is a 100-s example from the data collected at Ascension Island in the equatorial region during the past solar maximum (March 18, 2001) [24]. More than 25-dB fading, which can cause loss of lock of a receiver's carrier tracking channel, was frequently observed during this period.

fast reacquisition capability of an aviation receiver, which has been discussed in [28] and [29], we propose an additional performance requirement for future dual-frequency aviation receiver performance standards to increase the aviation availability under scintillation. The specific suggestion is given as follows.

> 2.1.1.9.2 Satellite Reacquisition Time under Very Short Signal Outages.
>
> For satellite signal outages of 1 second or less when the remaining satellites provide a GDOP of 6 or less, the equipment shall reestablish tracking the satellite within 1 second from the time the signal is reintroduced. This requirement applies to a satellite with the minimum signal power in the presence of interfering signals as described in Appendix C. Note: Equipment should be able to reestablish tracking satellites within 1 second from the time the signal is reintroduced under conditions of strong ionospheric scintillation that could cause short (1 second or less) and frequent (every 5 seconds) signal fades during solar maxima at equatorial latitudes.

The current Section 2.1.1.9 (Satellite Reacquisition Time) in the Wide Area Augmentation System (WAAS) [30] Minimum Operational Performance Standards (MOPS) [31], which is the performance standards for single-frequency GPS avionics, does not consider very short signal outages due to scintillation. (Performance standards for future dual-frequency GPS avionics is not yet available because dual-frequency aviation is expected in the 2020 time frame.) If a future dual-frequency MOPS also mandates only a 20-s reacquisition time after signal outages as in the current single-frequency MOPS, the availability of GPS-based aircraft landing guidance service down to 200 ft above the runway, which is also known as Localizer Performance with Vertical guidance (LPV) 200 [32], may be less than 50% during strong scintillation (see Section III).

This paper justifies that our proposal of a new receiver performance standard would significantly increase the availability of LPV-200 from less than 50% to more than 99% under strong scintillation in the dual-frequency era. In order to justify the expected availability benefit from the proposed standard, extensive parametric analyses are performed using a new integrity equation, an improved fading process model, and observed scintillation data from the past solar maximum.

A major integrity concern in the temporary single-frequency operation under a single-frequency loss due to scintillation is that the ionospheric delay cannot be directly measured until both frequencies are tracked again. In order to support this temporary single-frequency operation in the dual-frequency era, Section II proposes a new vertical protection level (VPL) equation bounding the uncertainty of ionospheric delay errors during a single-frequency loss. [VPL is the confidence bound of vertical position solution with 99.99999% probability. VPL must be less than vertical alert limit (VAL) for safe GPS-based aviation.]

Using this new VPL equation, the operational availabilities of LPV-200 under severe scintillation scenarios are evaluated in Section III. Since GPS L5 strong scintillation data are not yet available, this availability study utilizes the correlated fading process model proposed in [29]. The availability study in Section III justifies the effectiveness of the new VPL equation and the proposed performance standard, which would provide a more than 99% availability of LPV-200 under strong$>$ scintillation.

After the availability study, the sensitivity of the availability results to the fading rate of the L5 channel, which is not yet known, is parametrically evaluated in Section IV. The sensitivity of the availability results to the maximum bounded ionospheric gradient and satellite-to-satellite correlation is also studied. The fading process model originally proposed in [29] does not consider frequency-to-frequency correlation and satellite-to-satellite correlation simultaneously. The Appendix proposes an improved method to simulate doubly correlated fading processes, which is used for the sensitivity analysis. The sensitivity analysis in Section IV confirms that the most sensitive parameter affecting the availability is the reacquisition time of a receiver. Thus, the benefit of the proposed receiver performance standard mandating a fast reacquisition capability is further justified.

Based on the new VPL equation, availability study, and sensitivity analysis, Section V discusses our proposal of a new receiver performance standard in detail. This proposal is currently under discussion for inclusion in future dual-frequency aviation receiver performance standards.

II. New VPL Equation for Future Dual-Frequency GPS Aviation Under Ionospheric Scintillation

Ionospheric delay can be directly measured by future dual-frequency GPS avionics. Hence, the WAAS [30] geostationary satellites do not need to broadcast ionospheric delay estimations for these users. This is a significant benefit over current single-frequency aviation. The GNSS Evolutionary Architecture Study (GEAS) recommended architectures that will enable worldwide LPV service based on this dual-frequency upgrade of GPS satellites [4], [33]. Another expected benefit of dual-frequency operation is that it can provide a backup channel when one frequency is lost under ionospheric scintillation

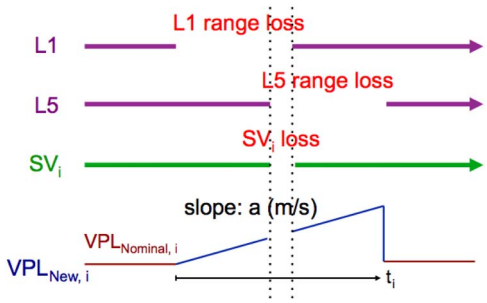

Fig. 2. Inflation of VPL to guarantee the integrity while ionospheric delay cannot be directly measured. The horizontal axis indicates the time. t_i is the elapsed time after a single-frequency loss of a satellite i. Satellite i is lost when both frequencies are lost. During a single-frequency loss, the pseudorange measurements from the other frequency can still be used for position calculations without compromising aviation integrity if the protection levels are properly inflated.

or radio-frequency interference (RFI) conditions. However, although a receiver can still measure pseudoranges from a remaining frequency during a single-frequency loss, the ionospheric delay cannot be directly measured until both frequencies are tracked again. Fig. 2 illustrates this situation. If both frequencies from a certain satellite channel are lost, no pseudorange measurement is available from the satellite; hence, the satellite is excluded from the position calculation. If a receiver tracks only the L5 frequency whereas the L1 frequency is lost after deep fading due to scintillation, for example, pseudorange measurements from L5 are still available although ionospheric delay cannot be measured by a single frequency alone.

Since ionospheric delay cannot be directly measured during a single-frequency loss, satellite-based augmentation systems (SBASs) such as WAAS in the United States may still need to broadcast ionospheric delay estimations in the dual-frequency era to support this temporary single-frequency operation mode. Although the broadcast ionospheric delay information is currently used for LPV service in the United States, the direct airborne measurement of ionospheric delay is much more desirable for worldwide LPV service. The WAAS broadcast information contains ionospheric delay amounts at each grid point only. Hence, a receiver interpolates the broadcast delays of nearby grid points for estimating a delay at a particular point of interest. A conservative estimate of error bounds on this interpolation is required to guarantee the aviation integrity, but it reduces the aviation availability. Moreover, GEAS architectures for worldwide LPV service do not necessarily require SBAS to guarantee the integrity. Therefore, another way to bound ionospheric delay errors during a single-frequency loss without relying on broadcast ionospheric delay estimations by SBAS is highly desired.

This section suggests a new VPL equation to bound the ionospheric uncertainty during brief single-frequency outages due to scintillation. For LPV-200 service, the protection level calculated by airborne avionics must bound the position errors with extremely high confidence. The uncertainty of the ionospheric delay error accumulates as the time advances after a single-frequency loss. Hence, if the protection level is properly inflated according to the elapsed time after a single-frequency loss, aircraft can be protected from this unknown ionospheric delay error.

The inflation of a new VPL is conceptually illustrated in Fig. 2 and defined as follows:

$$\mathrm{VPL_{New}} = \mathrm{VPL_{Nominal}} + \sum_{i=1}^{N} |S_{U,i} a t_i|$$

$$= K_v \sqrt{\sum_{i=1}^{N} S_{U,i}^2 \sigma_i^2} + \sum_{i=1}^{N} |S_{U,i} a t_i|. \qquad (1)$$

$\mathrm{VPL_{New},}_i$ in Fig. 2 is satellite i's contribution to $\mathrm{VPL_{New}}$ in (1). After a single-frequency loss of satellite i, the contribution to VPL from satellite i increases with a certain slope a as time t_i advances. Note that time t_i is zero when a receiver tracks both frequencies of satellite i. Once the receiver is again tracking both frequencies of satellite i, the new VPL drops to the nominal VPL value. The expression for the nominal case VPL, i.e., $\mathrm{VPL_{Nominal}} = K_v \sqrt{\sum_{i=1}^{N} S_{U,i}^2 \sigma_i^2}$, is given in [31, p. J-1]. As explained in [31], $S_{U,i}$ is "the partial derivative of position error in the vertical direction with respect to the pseudorange error on the ith satellite." The σ_i^2 is the variance of model distribution that overbounds the true error distribution on the ith satellite. Hence, $\sum_{i=1}^{N} S_{U,i}^2 \sigma_i^2$ is the "variance of model distribution that overbounds the true error distribution in the vertical axis." $K_v = 5.33$ is chosen to provide 10^{-7} bound (99.99999% confidence bound) of signal-in-space error, which is required for LPV-200. The inflated VPL term, i.e., $\sum_{i=1}^{N} |S_{U,i} a t_i|$, is added to this nominal case VPL under a single-frequency loss. The $a t_i$ is the deterministic model that overbounds the uncertainty of true ionospheric delay error on the ith satellite at a time t_i after a single-frequency loss. Inflation rate a must be selected to overbound the uncertainty of true ionospheric delay errors during a single-frequency loss. The t_i causes VPL to increase until it exceeds VAL at which point LPV-200 service is not available. (VAL of LPV-200 is 35 m.) The following section evaluates the availability of future dual-frequency GPS aviation under severe scintillation scenarios and shows the effectiveness of this new VPL equation.

III. Availability Analysis of Future Dual-Frequency GPS Aviation Under Severe Scintillation Scenarios

This section analyzes the availability of future dual-frequency GPS aviation under severe scintillation scenarios using the singly correlated fading process model proposed in [29]. (Later, a doubly correlated fading process model proposed in the Appendix will be used for the sensitivity analysis in Section IV-C.) In addition, the new VPL equation proposed in Section II is utilized. The parametric study of this section assesses the possible availability benefit from future dual-frequency aviation depending on the correlation level between L1 and L5 channels. The availability results will justify the effectiveness of the proposed receiver performance standard mentioned in Section I.

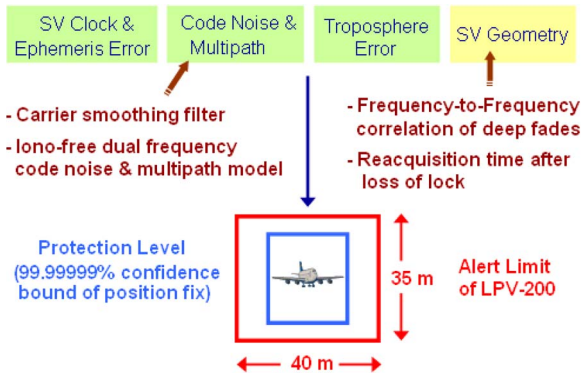

Fig. 3. Availability simulation procedure considering frequency-to-frequency correlation of deep fades under scintillation.

A. Availability Analysis Procedure

Fig. 3 illustrates the procedure to analyze the availability of future dual-frequency aviation under severe scintillation scenarios. For our availability analysis, protection levels are calculated at every second during 45 min of severe scintillation scenarios. If protection levels are lower than alert limits of LPV-200 (35 m vertical and 40 m horizontal), the LPV-200 service is "available" at the epoch. Satellite clock and ephemeris error [34], code noise and multipath, troposphere error, and satellite geometry are the parameters affecting the protection level calculation. Among the three GEAS architectures providing aviation integrity worldwide [4], GNSS integrity channel (GIC) architecture is assumed for our analysis. In the GIC architecture, integrity information is provided by a SBAS-like channel, but ionospheric delay estimations are not necessarily broadcast. A 1-m user range accuracy is assumed for satellite clock and ephemeris error. Iono-free dual-frequency code noise and multipath model based on the WAAS MOPS [31] is used. The carrier smoothing filter model in [28] considering shortened carrier smoothing time due to frequent signal loss is applied. The troposphere error model is from the WAAS MOPS. For satellite geometry, the GPS satellite constellation during the observed strong scintillation period at Ascension Island in 2001 is assumed as in [29] for the purpose of comparison. The reacquisition time of a receiver, or time to reestablish tracking and incorporate the lost channel into the position calculation after the signal is reintroduced, is a very important parameter affecting the availability during strong scintillation [28], [29]. In order to assess its importance in the dual-frequency operation, reacquisition time is also considered in our analysis.

There are three major differences in our availability analysis procedure from [29]. A correlated fading process model was developed in [29] to study satellite-to-satellite correlation of deep fades under strong scintillation. This previous study showed that the maximum satellite-to-satellite correlation observed during the strong scintillation at Ascension Island was only about 15%. Since the satellite-to-satellite correlation was very low, we ignore the satellite-to-satellite correlation in the first part of the availability analyses in this paper. Instead, the effect of frequency-to-frequency correlation on the availability is studied, which has not been previously analyzed. Previous studies such as [28] and [29] simply assumed that L1 and L5 channels are always lost simultaneously under scintillation (i.e., 100% frequency-to-frequency correlation).

Later, Section IV-C will discuss the effect of the ignored satellite-to-satellite correlation on the availability results. In order to analyze the effect, a doubly correlated fading process model is newly proposed. This improved fading process model is able to simulate both frequency-to-frequency correlation and satellite-to-satellite correlation simultaneously.

The remaining difference is that we use the new VPL equation in (1) to guarantee the integrity during a temporary single-frequency operation. Hence, a receiver does not rely on broadcast ionospheric delay estimations, which may not be available in future GEAS architectures. The MATLAB Algorithm Availability Simulation Tool [35] is modified to incorporate these settings.

Before discussing the availability results, it would be informative to briefly review the correlated fading process model proposed in [29], which is necessary to understand the newly proposed doubly correlated fading process model in the Appendix. Seo *et al.* [29] discussed a weakness of the conventional definition of sample correlation coefficient in the following for GPS aviation study under scintillation:

$$\hat{\rho} = \frac{\sum_i (x_i - \bar{x})(y_i - \bar{y})}{\sqrt{\sum_i (x_i - \bar{x})^2}\sqrt{\sum_i (y_i - \bar{y})^2}}. \tag{2}$$

The x_i and y_i are the C/N_0 sample points of two different channels, and $\bar{x}$ and $\bar{y}$ are mean values. This sample correlation coefficient evaluates the similarity of two C/N_0 time series, but it does not explain how often both channels fade simultaneously. A better definition of correlation coefficient for GPS aviation study was proposed and mathematically justified. If we follow the definition of correlation coefficient in [29] for studying frequency-to-frequency correlation of deep fades, the sample correlation coefficient between L1 and L5 channels is expressed as in (3), shown at the bottom of the page. (T is an observation time window.)

This correlation coefficient explains how often L1 and L5 channels experience deep fading simultaneously. If the correlation coefficient is 1, for example, it implies that L1 and L5 channels always experience deep fading simultaneously. In this case, L1 and L5 channels could experience simultaneous loss of lock due to simultaneous deep fading; hence, the backup frequency may not improve the availability. Since this definition of a correlation coefficient is exactly what interests us, we follow this definition in this paper.

$$\hat{\rho}(T) = \frac{\text{Number of simultaneous deep fades between L1 and L5 channels}}{\sqrt{\text{Number of deep fades of L1 channel}}\sqrt{\text{Number of deep fades of L5 channel}}} \tag{3}$$

The correlated fading process model in [29] also complies with this definition of correlation coefficient. It was shown that the counting process of number of deep fades could be conservatively modeled with a Poisson process with an appropriate rate [29]. Using the property that a combination of two Poisson processes is still a Poisson process with added rates [36], two correlated Poisson processes modeling correlated fading processes can be generated with any correlation coefficient (see [29] for complete explanation). This previous study generated fading processes with satellite-to-satellite correlation, but the same method can be applied to generate fading processes with frequency-to-frequency correlation. (However, satellite-to-satellite correlation and frequency-to-frequency correlation cannot be simulated simultaneously by this previous model. We overcome this limitation by a new fading process model proposed in the Appendix.) The correlated fading process model generates instances of loss of lock using a mathematical model based on statistical observations, but it does not consider the physics of scintillation.

Note that the rate of L1 fading (the number of L1 deep fades per unit time; equivalently, the number of L1 losses of lock per unit time if a receiver is conservatively assumed to lose lock at every deep fade as in this paper), λ_{L1}, for our availability simulation is obtained from the Ascension Island data (i.e., $\lambda_{\mathrm{L1}} = 1/9.71$ s) as in [29]. However, the rate of L5 fading is not yet known from real strong scintillation data. According to Fremouw *et al.* [37], the amplitude scintillation index (S_4 index) of the L5 frequency is expected to be larger than the S_4 index of the L1 frequency, i.e.,

$$S_{4,\,\mathrm{L5}} = S_{4,\,\mathrm{L1}} \left(\frac{f_{\mathrm{L1}}}{f_{\mathrm{L5}}} \right)^{1.5} = 1.55 S_{4,\,\mathrm{L1}}. \tag{4}$$

However, (4) does not relate the rates of losses of lock of the L1 and L5 channels. Although the signal fluctuations of the L5 channel could be worse than the L1 signal fluctuations, the higher power and better code structure of the L5 signal [38] would reduce the chance of loss of lock of the L5 tracking channel. We first will assume that the L5 fading rate (the number of L5 losses of lock per unit time) is the same as the L1 fading rate in Section III-B. Later, Section IV-A will evaluate the effect of higher L5 fading rates on the availability results.

B. Availability Results Depending on Ionospheric Error Bound During a Single-Frequency Loss

Depending on the selection of inflation rate a in Fig. 2, three different approaches to bounding the ionospheric delay error during a single-frequency loss are evaluated in this section. Under each approach, availability results will be presented with two parameters: the correlation coefficient between L1 and L5 fading channels (every 0.1, from 0 to 1), and the reacquisition time of a receiver (every 1 s, from 0 to 10 s).

The most conservative approach assumes $a = \infty$, which tends the contribution of satellite i to VPL, i.e., $|S_{U,\,i} a t_i|$, toward infinity when satellite i loses either frequency (i.e., when $t_i > 0$). In other words, a receiver does not trust range measurements from a satellite if the receiver loses either the L1 or L5 channel of the satellite because the ionospheric delay cannot be directly measured. Since a satellite is excluded from the position calculation whenever either frequency is lost in this extremely conservative approach, the aviation integrity is always guaranteed. However, the aviation availability would be very low under severe scintillation scenarios, as shown in Fig. 4. Even a reacquisition time of 1 s cannot provide a high availability ($> 99\%$). As noted in Fig. 4, a higher correlation between the L1 and L5 channels gives a better availability in this most conservative approach. (A higher frequency-to-frequency correlation means that losses of the L1 and L5 channels occur simultaneously with a higher probability.) This is because a receiver does not use range measurements for position calculations unless dual-frequency measurements are available. Hence, if a receiver were to lose one frequency followed by the other, the total duration of the satellite loss would be extended. Therefore, it is better to lose both frequencies together instead of losing one frequency after the other if the fading rates of two frequency channels are fixed.

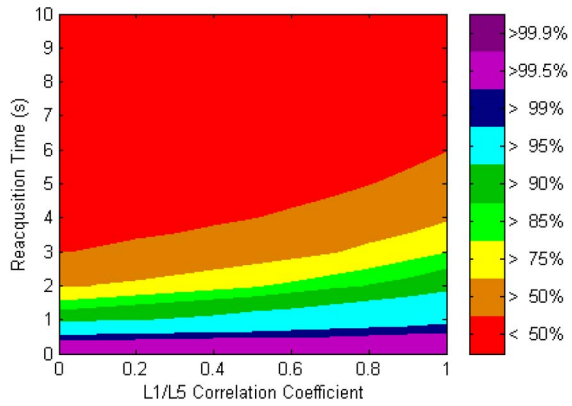

Fig. 4. Availability contour of LPV-200 under severe scintillation scenarios and the most conservative approach ($a = \infty$) to bound the ionospheric delay error during a single-frequency loss. a is the inflation rate in (1). A higher frequency-to-frequency correlation gives a better availability in this case if the fading rates of the L1 and L5 channels are fixed.

The availability in Fig. 4 is obtained under severe scintillation scenarios generated by the fading process model. The scintillation scenarios are based on the worst 45-min scintillation of a campaign at Ascension Island during the past solar maximum as in [29], but the scenarios represent worse situations than the observation. In the scenarios, all eight satellite channels are assumed to experience the very frequent deep fades for the whole 45 min, and a receiver is assumed to lose its tracking lock with a 100% probability at every deep fade. The deep fades of the L1 and L5 channels of each satellite are assumed to be correlated with a given correlation coefficient for the whole period.

Another extreme approach to bound ionospheric delay error during a temporary single-frequency operation is to assume $a = 0$. Since fading duration is very brief (mostly less than 1 s [23], [24]), the ionospheric delay error may not grow significantly during this short period. Hence, a receiver may use the most recent ionospheric delay measurement during the brief period of single-frequency loss. In this most optimistic approach, a receiver fully relies on the pseudorange measurements from a single frequency, and the most recent ionospheric

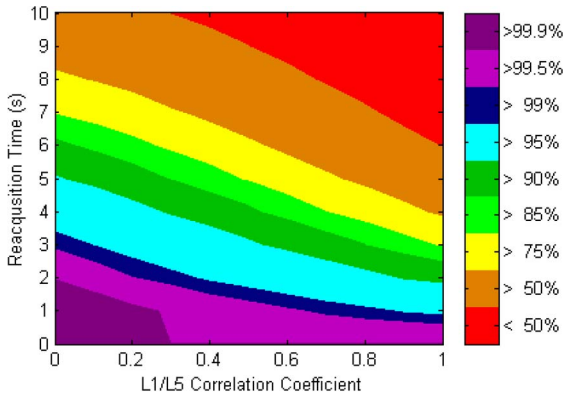

Fig. 5. Availability contour of LPV-200 under severe scintillation scenarios and the most optimistic approach ($a = 0$, i.e., the ionospheric uncertainty does not grow with time) to bound the ionospheric delay error during a single-frequency loss.

delay measurement when the other frequency is briefly lost. The availability of LPV-200 under this approach is presented in Fig. 5. Now, the receiver takes the full benefit from the backup frequency. (Hence, a lower frequency-to-frequency correlation of deep fades provides a better availability as expected.) Although the actual correlation level between the L1 and L5 channels should be validated based on extensive scintillation data to be collected during this solar maximum from various sensor networks such as [39], Fig. 5 parametrically illustrates the expected availability levels depending on a correlation coefficient and a receiver's reacquisition time under the severe scintillation scenarios. In this case, a reacquisition time of 1 s provides more than 99% availability if the L1/L5 correlation is less than 80%.

Two extreme approaches for bounding the ionospheric delay error were discussed. The most conservative approach is too conservative to provide high availability even if the integrity is perfectly guaranteed. The most optimistic approach gives high availability, but it may be too optimistic to guarantee the integrity. In the equatorial area, scintillation often accompanies depletions, i.e., regions of steep ionospheric gradient. Thus, sudden large changes in ionospheric delay are expected to occur simultaneously with strong scintillation. Hence, this expected steep ionospheric gradient should be properly bounded by a nonzero inflation rate a (see Fig. 2).

In the third approach, the steepest observed ionospheric gradient and the worst case geometry of the gradient and the satellites are assumed for guaranteeing the integrity. According to Datta-Barua *et al.* [40], 425 mm/km was the largest observed gradient in slant ionospheric delay at the L1 frequency within the conterminous United States (CONUS). Under the same ionospheric condition, ionospheric gradient at the L5 frequency would be $(f_{L1}^2/f_{L5}^2) \times 425$ mm/km $= 762$ mm/km. The worst case combination of geometries is illustrated in Fig. 6. If a satellite and a plane move in the same direction and if the steepest ionospheric gradient moves toward the plane, the relative speed of the ionospheric pierce point with respect to the ionospheric gradient could be as high as 950 m/s. As a result, the temporal pseudorange error can grow as fast as 0.40 m/s at L1 and 0.72 m/s at L5. Hence, if $a = 0.72$ m/s is selected in (1) to be conservative, the ionospheric delay error due to the

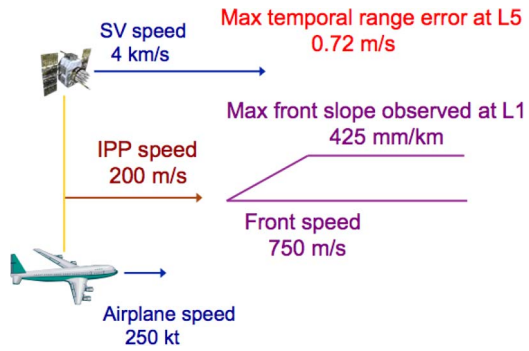

Fig. 6. Maximum temporal pseudorange error (0.72 m/s) under the worst case combination of the geometry of a plane, a GPS satellite, and the maximum ionospheric front slope observed in CONUS. Maximum aircraft speed is 250 kn for initial approach and 230 kn for final approach (see [41, Tables I-4-1-2]). Maximum ionospheric front speed in the CONUS threat model is 750 m/s [40].

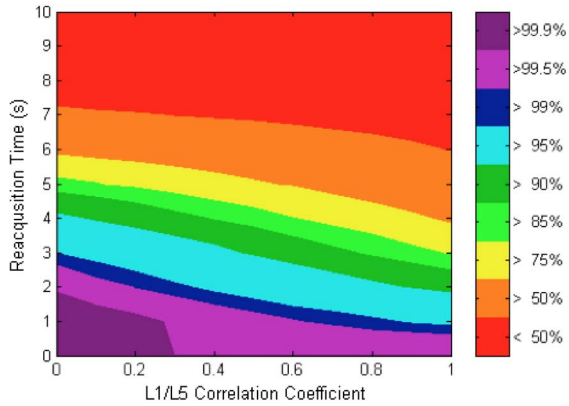

Fig. 7. Availability contour of LPV-200 under severe scintillation scenarios and the maximum observed ionospheric gradient and the worst case geometries. $a = 0.72$ m/s is selected to bound the maximum temporal pseudorange error caused by this worst case condition.

maximum observed gradient under the worst case geometries for all satellites in view will be properly bounded.

The availability contour with $a = 0.72$ m/s is shown in Fig. 7. Compared with the most optimistic approach of Fig. 5, there is not much difference in availabilities if a receiver reacquires the lost channel within 3 s. A certain model of an aviation receiver already demonstrated fast reacquisition capability under scintillation (less than 2 s in 91% cases during a campaign in Brazil [28]). Therefore, a high availability with the required integrity would be attainable even under the severe scintillation scenarios if the new VPL equation in (1) is applied and inflation rate a is properly selected.

IV. Sensitivity Analyses of the Availability Results

This section analyzes the sensitivity of the availability results in Section III to various parameters expected to impact the availability. The sensitivity analysis of this section will confirm that the most sensitive parameter affecting the availability is the reacquisition time of a receiver. Thus, the high availability provided by the fast reacquisition capability of the proposed standard would not be significantly impacted by the uncertainty of other parameters.

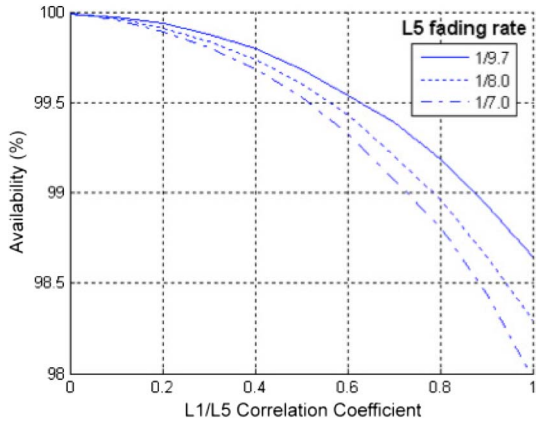

Fig. 8. Availability of LPV-200 with various L5 fading rates (1/9.7, 1/8, and 1/7 losses of lock per second). The L1 fading rate is fixed to 1/9.7 as observed during the strong scintillation of the previous solar maximum [29]. Reacquisition time is assumed 1 s.

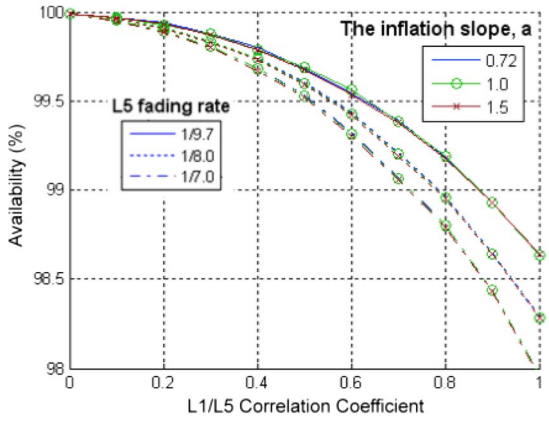

Fig. 9. Availability of LPV-200 with various inflation rates a of the new VPL equation (0.72, 1, 1.5 m/s). As in Fig. 8, three L5 fading rates (1/9.7, 1/8, and 1/7 losses of lock per second) are considered for each value of a. Reacquisition time is assumed 1 s.

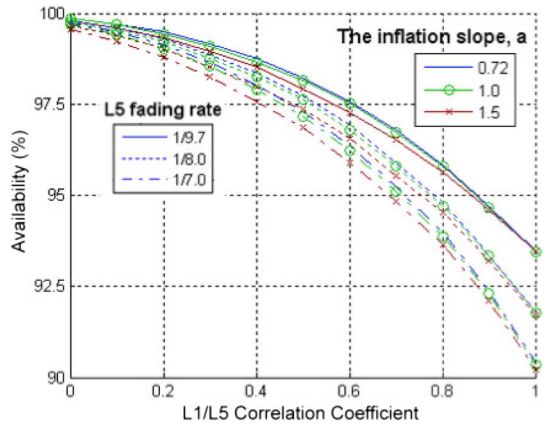

Fig. 10. Availability of LPV-200 with a reacquisition time of 2 s. Other conditions are the same as in Fig. 9.

A. Sensitivity to the Fading Rate of the L5 Channel

Section III assumed that the fading rate of the L5 channel would be the same as the fading rate of the L1 channel. As discussed in Section III-A, this assumption is probable, but it is not yet supported by real scintillation data. Therefore, this section evaluates the sensitivity of the availability results of Section III to the uncertainty of the L5 fading rate.

As the L5 fading rate increases from 1/9.7 losses of lock per second to 1/7, for example, the expected availability slightly decreases (see Fig. 8). (Note that the 1/7 losses of lock per second is 1.38 times higher than the worst rate of L1 fading in the Ascension Island data, which is 1/9.7. Thus, this value provides a margin for the uncertainty of the L5 fading rate.) However, if a receiver can reacquire the lost channel within 1 s as in Fig. 8, more than 98% availability is attainable even under the 100% correlation between L1 and L5 and the simulated severe scintillation scenarios. It is interesting to note that the availability decrease due to the increased L5 fading rate being less than 1 percentage point. As in Fig. 7, the new VPL of (1) with $a = 0.72$ m/s is used for this analysis. Compared with Fig. 7, it is evident that availability is much more sensitive to the reacquisition time than to the L5 fading rate.

B. Sensitivity to the Maximum Bounded Ionospheric Gradient

The sensitivity study of Fig. 8 assumed that $a = 0.72$ m/s can bound the uncertainty of the ionospheric delay error during a single frequency loss. As explained in Fig. 6, this is true for the steepest ionospheric gradient observed in CONUS and the worst case geometry. However, an even steeper ionospheric gradient may occur in the equatorial area during high solar activity in the future. Thus, ionospheric gradients should be continuously monitored in the service area, and the up-to-date steepest gradient value must be applied to guarantee the aviation integrity [42]. The inflation rate a must be updated accordingly. As of this writing, $a = 0.72$ m/s is a suggested value for the new VPL equation.

If an even steeper ionospheric gradient were to occur in the future, $a = 1$ m/s or even $a = 1.5$ m/s would be necessary to bound the uncertainty. If $a = 1$ m/s is used, for example, it can protect against a 1.4 times steeper ionospheric gradient (i.e., 590 mm/km at L1) than the steepest observed gradient in CONUS. The sensitivity of the availability results to the maximum bounded ionospheric gradient is studied with $a =$ 0.72, 1, and 1.5 m/s (see Fig. 9). Interestingly, the availability result is not very sensitive to the maximum bounded gradient if a receiver can reacquire a lost channel within 1 s. The availability decrease due to the increased a values shown in Fig. 9 being less than 0.1 percentage point.

Even with $a = 1.5$ m/s, which can protect against a twice steeper ionospheric gradient than the steepest observed value, the additional contribution of a satellite to VPL, which is at_i in (1), grows up to 1.5 m. This value is not very significant compared with the VAL of LPV-200, which is 35 m. Hence, the importance of a short reacquisition time under strong scintillation is further emphasized. Similar sensitivity results in the case of a reacquisition time of 2 s are shown in Fig. 10.

C. Impact of Satellite-to-Satellite Correlation of Deep Fades

The method to generate correlated fading processes proposed in [29] is useful to simulate the instances of loss of lock during arbitrary severe scintillation with any fading rate and correlation coefficient between two channels. However, the

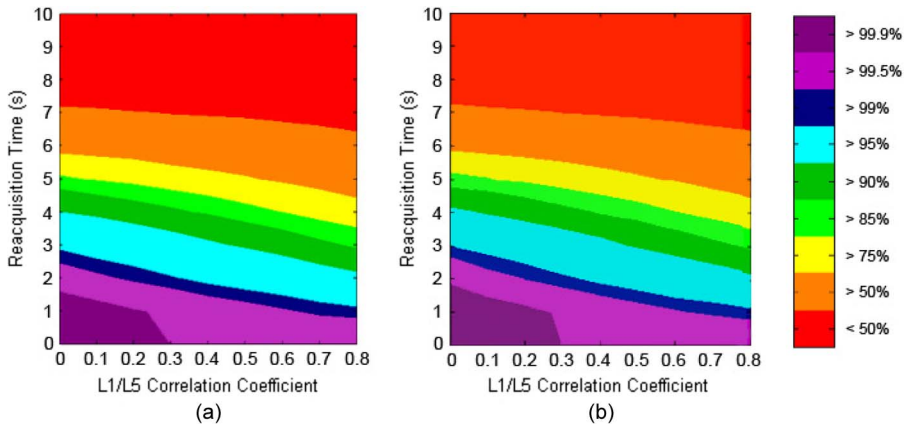

Fig. 11. (a) Availability contour of LPV-200 with the consideration of both satellite-to-satellite correlation (15% correlation) and frequency-to-frequency correlation (every 10%, from 0% to 80%). The 15% satellite-to-satellite correlation does not noticeably change the availability result in Fig. 7. (b) Availability contour extracted in Fig. 7 for frequency-to-frequency correlation from 0% to 80%. This figure is for a side-by-side comparison.

method cannot simulate doubly correlated fading processes. Imagine two GPS satellites with L1 and L5 channels. The L1 channel of satellite 1 and the L1 channel of satellite 2 can be correlated (satellite-to-satellite correlation), for example. Similarly, the L1 and L5 channels of satellite 1 can be also correlated (frequency-to-frequency correlation). The method in [29] cannot consider both satellite-to-satellite correlation and frequency-to-frequency correlation at the same time. Hence, the impact of frequency-to-frequency correlation was studied with the assumption of 0% correlation between satellites in previous sections. Although the satellite-to-satellite correlation was ignored in the availability analysis so far, it was justified because the level of observed satellite-to-satellite correlation during strong scintillation was very low [29].

However, it will be still informative to study whether the effect of satellite-to-satellite correlation on the availability results of this paper is negligible. A new method to generate doubly correlated fading processes is proposed and explained in the Appendix. This method can consider both satellite-to-satellite correlation and frequency-to-frequency correlation simultaneously. A caveat of this method is that the sum of the satellite-to-satellite correlation coefficient and the frequency-to-frequency correlation coefficient cannot be greater than 1 (see Appendix). Hence, if a satellite-to-satellite correlation coefficient of 0.15 is assumed as observed during the past solar maximum [29], a frequency-to-frequency correlation coefficient larger than 0.85 cannot be simulated using this method. This section assumes the satellite-to-satellite correlation coefficient of 0.15 and evaluates the availability of LPV-200 for frequency-to-frequency correlation coefficients from 0 to 0.80 (every 0.10).

As shown in Fig. 11(a), the availability contour does not present a significant difference from the availability contour in Fig. 7, which ignored the effect of satellite-to-satellite correlation. Therefore, the 15% satellite-to-satellite correlation observed during the past solar maximum does not significantly impact the availability of LPV-200. The effect of frequency-to-frequency correlation is more important, and the effect of a receiver's reacquisition time is paramount.

As explained in Section III-B, the severe scintillation scenarios simulated for our availability study are much worse

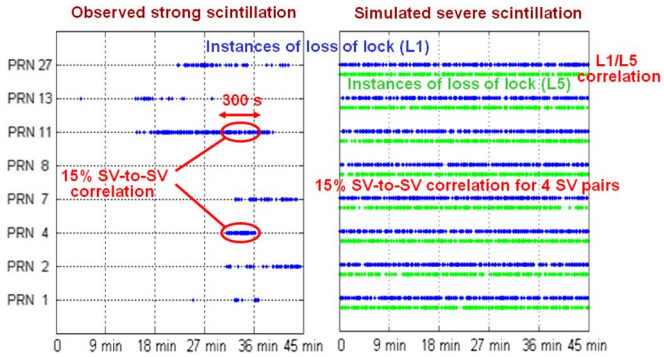

Fig. 12. Comparison between the observed strong scintillation at Ascension Island in [29] and the simulated severe scintillation for our analyses. Each dot indicates the instance of loss of lock of the corresponding channel (a blue dot for the L1 channel and a green dot for the L5 channel). During the simulated scintillation, a receiver loses lock on L1 and L5 very frequently for the whole 45 min.

than the real observations during the past solar maximum. Fig. 12 compares the instances of loss of lock during the observed strong scintillation period and the simulated severe scintillation period. During the real scintillation from the past solar maximum in [29], seven GPS satellites lost lock for fractions of 45 min. However, during the simulated scintillation used for our availability analysis, all eight satellites frequently lose lock for the whole 45 min, which is much worse than the real scintillation. Although the real scintillation data was recorded by an L1-only receiver, correlated L1 and L5 channels are generated for the dual-frequency simulation. In addition to this frequency-to-frequency correlation, 15% satellite-to-satellite correlation is applied to each satellite pair (i.e., total four pairs, or eight satellites) using the method in the Appendix during the whole 45 min. In the real scintillation data, the 15% worst case correlation occurred for only one satellite pair during the worst 300 s only [29].

Even with these severe scintillation scenarios and the conservative steps throughout the analysis, more than 99% availability of LPV-200 is achievable if a receiver can reacquire the lost channel within 1 s and the L1/L5 correlation coefficient is less than 0.8 [see Fig. 11(a)]. (The availability analyses in this paper consider a worst 45-min scintillation of a day. Therefore, the

99% availability during the worst 45 min of a day implies that the average operational availability for 24 h of solar maxima will be much higher than 99%.) El-Arini *et al.* [43] reported the correlation coefficient of about 0.7 between L1 and L2 channels. Since the frequency separation between L1 and L5 is larger than the separation between L1 and L2, the correlation coefficient between L1 and L5 is expected to be less than 0.7. However, direct application of this previous correlation result is not very meaningful because the definition of correlation coefficient in [43], i.e., (2), is different from the definition used in this paper, i.e., (3). Since L5 strong scintillation data are not yet available, the true correlation level between L1 and L5 should be confirmed based on extensive scintillation data to be collected during this solar maximum.

V. Strategy to Achieve High Aviation Availability Under Strong Scintillation

Although the importance of a fast reacquisition capability of an aviation receiver under strong scintillation was previously discussed in [28] and [29], the correlated signal fades between two frequency channels of future dual-frequency aviation have not been previously analyzed. This paper shows that a fast reacquisition capability can provide higher availability for future dual-frequency GPS aviation. This is an expected result, but it is interesting to note that the attainable availability level would be as high as 99% if the proposed receiver standard is applied.

The current aviation receiver performance standards (WAAS MOPS [31]) specifies up to 20 s of reacquisition time when signal outages are less than 30 s. Since a reacquisition time of 20 s may result in less than 50% availability of LPV-200 during strong scintillation, we previously suggested to lower the upper bound of allowed reacquisition time to 1–2 s [28]. As aforementioned, a certain model of an aviation receiver already demonstrated fast reacquisition capability under scintillation (less than 2 s in 91% cases during a campaign in Brazil [28]). The signal outages due to scintillation are much briefer than the 30-s outages due to RFI, which are considered in the current MOPS requirement. Under brief outages due to scintillation (mostly less than 1 s [23], [24]), there is no compelling reason for a receiver to take 20 s to reacquire the lost channel, although the reacquisition time of 20 s is allowed by the current requirement. However, the receiver could take longer time to reestablish tracking after longer outages due to RFI (see [31, Sec. 2.1.1.9; App. C]). Thus, lowering the upper bound of allowed reacquisition time regardless of outage duration may not be practical. As a better suggestion, we propose a separate requirement mandating fast reacquisition (1 s) under very brief outages (less than 1 s) due to scintillation while keeping the current requirement allowing reacquisition time of 20 s after outages of less than 30 s due to RFI. With these two separate requirements, a receiver algorithm has flexibility to respond differently to different outage durations.

The specific suggestions for future dual-frequency aviation receiver performance standards are given as follows. A preliminary version of these requirements was presented at a standards committee working group meeting (RTCA Special Committee-159 Working Group-2 meeting).

2.1.1.9 Satellite Reacquisition Time.

2.1.1.9.1 Satellite Reacquisition Time under Short Signal Outages.

For satellite signal outages of 30 seconds or less when the remaining satellites provide a GDOP of 6 or less, the equipment shall reacquire the satellite within 20 seconds from the time the signal is reintroduced. This requirement applies to a satellite with the minimum signal power in the presence of interfering signals as described in Appendix C. Note: For SBAS satellites, the momentary loss of signal for less than 4 seconds does not obviate any of the time out intervals defined for SBAS data in Section 2.1.1.4.9. The equipment can continue to use data until it times out.

2.1.1.9.2 Satellite Reacquisition Time under Very Short Signal Outages.

For satellite signal outages of 1 second or less when the remaining satellites provide a GDOP of 6 or less, the equipment shall reestablish tracking the satellite within 1 second from the time the signal is reintroduced. This requirement applies to a satellite with the minimum signal power in the presence of interfering signals as described in Appendix C. Note: Equipment should be able to reestablish tracking satellites within 1 second from the time the signal is reintroduced under conditions of strong ionospheric scintillation that could cause short (1 second or less) and frequent (every 5 seconds) signal fades during solar maxima at equatorial latitudes.

The requirement in the proposed Section 2.1.1.9.1 (Satellite Reacquisition Time under Short Signal Outages) is the same as the requirement in the current Section 2.1.1.9 (Satellite Reacquisition Time) in the WAAS MOPS [31]. The proposed Section 2.1.1.9.2 (Satellite Reacquisition Time under Very Short Signal Outages) specifies an additional requirement for a scintillation environment. Basically, the current "Satellite Reacquisition Time" requirement is split into two different requirements, which consider both "Satellite Reacquisition Time under Short Signal Outages" for RFI (a reacquisition time limit of 20 s for outages of 30 s or less) and "Satellite Reacquisition Time under Very Short Signal Outages" for scintillation (a reacquisition time limit of 1 s for outages of 1 s or less). A receiver should properly manage an RFI condition with longer outages and a scintillation condition with shorter outages accordingly.

This additional requirement is under discussion for inclusion in future dual-frequency aviation receiver performance standards. Aviation receiver manufacturers are also involved in the discussion. As the current reacquisition time test specified in the WAAS MOPS (Section 2.5.6 Satellite Reacquisition Time Test of [31]), receiver performance under very short and frequent signal outages can be also tested using an RF simulator. If aviation receiver manufacturers have difficulties satisfying the deterministic limit of a reacquisition time of 1 s after an outage of less than 1 s and other MOPS requirements simultaneously, a probabilistic requirement (e.g., a reacquisition time of 1 s with more than 95% probability and a reacquisition time of 2 s with more than 99% probability) can be also considered. Since this paper has not performed availability analysis with probabilistic reacquisition times, further analyses are required if a probabilistic requirement is considered.

VI. Conclusion

This paper proposed a receiver performance standard for future dual-frequency GPS aviation to improve the aviation availability under strong ionospheric scintillation. Since shortening the reacquisition time, which is required in the proposed standard, significantly improves the availability against scintillation in every scenario in this paper, the effectiveness of the proposed standard was justified.

In order to guarantee aviation integrity during a single-frequency loss, the uncertainty of ionospheric delay error must be properly bounded. A new VPL equation to protect against the ionospheric delay error was proposed, and three different approaches to bounding the uncertainty were compared. Two extreme approaches [i.e., the inflation rate $a = \infty$ or $a = 0$ in (1)] are either too conservative or too optimistic. By a proper selection of the inflation rate, high availability of LPV-200 is attainable while still guaranteeing integrity.

If the L5 fading rate is higher than the worst case L1 fading rate observed at Ascension Island [29], the availability would be slightly reduced. However, the L5 fading rate is not a very sensitive parameter, particularly if compared with the sensitivity to the reacquisition time. The sensitivity study showed that high availability is attainable even under the ionospheric gradient that is three times steeper than the steepest gradient observed in CONUS if a receiver can reestablish tracking within 1 s after a very brief outage. The impact of the ignored satellite-to-satellite correlation is assessed via the proposed doubly correlated fading process model. The result confirmed that the low satellite-to-satellite correlation during strong scintillation does not meaningfully change the availability results.

Due to the uncertainty of ionospheric gradient, L1 and L5 fading rate, satellite-to-satellite correlation, and frequency-to-frequency correlation, we performed parametric study with various scenarios based on the very limited observations from the past solar maximum. Future data collection campaigns through this solar maximum will provide a better estimation of those parameters. Consequently, the availability of LPV-200 can be better estimated within the parametric space of this paper.

Under the current standards [31] of allowing a reacquisition time of 20 s, a receiver may perform extensive safety checks even after a very brief outage, but it is not clear that this requirement is strictly necessary. As nearly demonstrated by a certain aviation receiver [28], the new requirement of a reacquisition time of 1 s after an outage of less than 1 s is expected to be achievable by a software modification to avoid a full safety check for very brief outages. Receiver manufacturers are evaluating whether there is a negative impact on L1 interference mitigation by satisfying this new requirement. After close discussion with the manufacturers, the standards committee will recommend specific requirements and test procedures to overcome ionospheric scintillation for worldwide dual-frequency GPS aviation expected in the 2020 time frame.

Appendix A
Doubly Correlated Fading Process Model

This appendix proposes a model to generate doubly correlated fading processes. This model expands the correlated

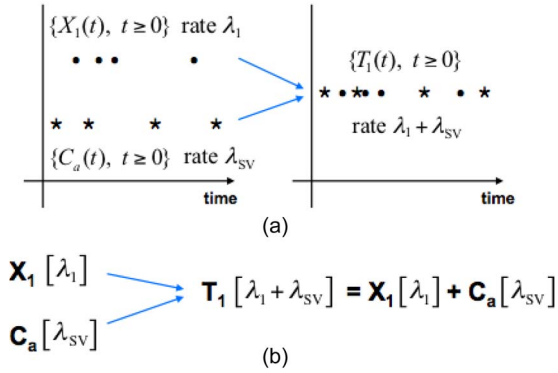

Fig. 13. Simplified notation for combining two Poisson processes. The dots in (a) indicate the instances of arrivals of Poisson process $\{X_1(t), t \geq 0\}$ of rate λ_1. Similarly, the stars in (a) indicate the instances of arrivals of Poisson process $\{C_a(t), t \geq 0\}$ of rate λ_{SV}. If these two Poisson processes are combined together as in (a), the resulting process $\{T_1(t), t \geq 0\}$ is still a Poisson process of added rate $\lambda_1 + \lambda_{\mathrm{SV}}$ [36]. A simplified notation in (b) is used in the Appendix.

$$\mathbf{L_{1,SV1}}\left[\lambda_1+\lambda_{\mathrm{SV}}+\lambda_{15}\right] = \mathbf{X_1}\left[\lambda_1\right] + \mathbf{C_a}\left[\lambda_{\mathrm{SV}}\right] + \mathbf{C_c}\left[\lambda_{15}\right]$$

$$\mathbf{L_{5,SV1}}\left[\lambda_5+\lambda_{\mathrm{SV}}+\lambda_{15}\right] = \mathbf{X_5}\left[\lambda_5\right] + \mathbf{C_b}\left[\lambda_{\mathrm{SV}}\right] + \mathbf{C_c}\left[\lambda_{15}\right]$$

$$\mathbf{L_{1,SV2}}\left[\lambda_1+\lambda_{\mathrm{SV}}+\lambda_{15}\right] = \mathbf{Y_1}\left[\lambda_1\right] + \mathbf{C_a}\left[\lambda_{\mathrm{SV}}\right] + \mathbf{C_d}\left[\lambda_{15}\right]$$

$$\mathbf{L_{5,SV2}}\left[\lambda_5+\lambda_{\mathrm{SV}}+\lambda_{15}\right] = \mathbf{Y_5}\left[\lambda_5\right] + \mathbf{C_b}\left[\lambda_{\mathrm{SV}}\right] + \mathbf{C_d}\left[\lambda_{15}\right]$$

Fig. 14. Generation of four doubly correlated Poisson processes $L_{1,\mathrm{SV1}}$, $L_{5,\mathrm{SV1}}$, $L_{1,\mathrm{SV2}}$, and $L_{5,\mathrm{SV2}}$ from eight independent Poisson processes X_1, C_a, Y_1, X_5, C_b, Y_5, C_c, and C_d. The combination of two Poisson processes notated with the "+" sign follows the way of Fig. 13.

Poisson process model in [29] and simulates satellite-to-satellite correlation and frequency-to-frequency correlation of deep fades simultaneously. Before explaining our model, Fig. 13 defines the notation used in this appendix. $\{X_1(t), t \geq 0\}$ in Fig. 13(a) is a Poisson process of rate λ_1, and $\{C_a(t), t \geq 0\}$ is a Poisson process of rate λ_{SV}. When these two Poisson processes are combined together, the resulting process $\{T_1(t), t \geq 0\}$ is still a Poisson process of added rate [36]. In Fig. 13(b), a simplified notation X_1 is used for a Poisson process $\{X_1(t), t \geq 0\}$ and its rate is shown in square brackets as $[\lambda_1]$, for example. We denote the combination of two Poisson processes with a "+" sign. Hence, the Poisson process $\{T_1(t), t \geq 0\}$ is expressed as $T_1\ [\lambda_1 + \lambda_{\mathrm{SV}}] = X_1[\lambda_1] + C_a\ [\lambda_{\mathrm{SV}}]$ with its rate $[\lambda_1 + \lambda_{\mathrm{SV}}]$ in square brackets. Since $\{T_1(t), t \geq 0\}$ is a Poisson process of rate $\lambda_1 + \lambda_{\mathrm{SV}}$, $T_1(t)$ for a given t is a Poisson random variable with a mean and variance $(\lambda_1 + \lambda_{\mathrm{SV}})t$ [36].

Following this notation, Fig. 14 illustrates the procedure to obtain four doubly correlated Poisson processes $\{L_{1,\mathrm{SV1}}(t), t \geq 0\}$, $\{L_{5,\mathrm{SV1}}(t), t \geq 0\}$, $\{L_{1,\mathrm{SV2}}(t), t \geq 0\}$, and $\{L_{5,\mathrm{SV2}}(t), t \geq 0\}$ with rates $\lambda_1 + \lambda_{\mathrm{SV}} + \lambda_{15}$, $\lambda_5 + \lambda_{\mathrm{SV}} + \lambda_{15}$, $\lambda_1 + \lambda_{\mathrm{SV}} + \lambda_{15}$, and $\lambda_5 + \lambda_{\mathrm{SV}} + \lambda_{15}$, respectively. Once we generate three independent Poisson processes X_1, C_a, and C_c with corresponding rates in square brackets, the Poisson process $L_{1,\mathrm{SV1}}$ can be obtained by combining these three Poisson processes, i.e., $L_{1,\mathrm{SV1}} = X_1 + C_a + C_c$.

Similarly, $L_{5,\mathrm{SV1}}$, $L_{1,\mathrm{SV2}}$, and $L_{5,\mathrm{SV2}}$ can be also obtained. Since $L_{1,\mathrm{SV1}}$, $L_{5,\mathrm{SV1}}$, $L_{1,\mathrm{SV2}}$, and $L_{5,\mathrm{SV2}}$ are Poisson processes, $L_{1,\mathrm{SV1}}(t)$, $L_{5,\mathrm{SV1}}(t)$, $L_{1,\mathrm{SV2}}(t)$, and $L_{5,\mathrm{SV2}}(t)$ for a given time t are Poisson random variables with means and variances of $(\lambda_1+\lambda_{\mathrm{SV}}+\lambda_{15})t$, $(\lambda_5+\lambda_{\mathrm{SV}}+\lambda_{15})t$, $(\lambda_1+\lambda_{\mathrm{SV}}+\lambda_{15})t$, and $(\lambda_5+\lambda_{\mathrm{SV}}+\lambda_{15})t$, respectively.

Now, the covariance between two Poisson random variables $L_{1,\mathrm{SV1}}(t)$ and $L_{5,\mathrm{SV1}}(t)$ can be calculated. If the Poisson processes X_1, X_5, C_a, C_b, and C_c are all independently generated, the Poisson random variables $X_1(t)$, $X_5(t)$, $C_a(t)$, $C_b(t)$, and $C_c(t)$ for a given t are all independent. Hence

$$\begin{aligned}
&E\left[L_{1,\mathrm{SV1}}(t)\,L_{5,\mathrm{SV1}}(t)\right]\\
&\quad=E\left[\{X_1(t)+C_a(t)+C_c(t)\}\{X_5(t)+C_b(t)+C_c(t)\}\right]\\
&\quad=E[X_1(t)X_5(t)+X_1(t)C_b(t)+X_1(t)C_c(t)\\
&\qquad+C_a(t)X_5(t)+C_a(t)C_b(t)+C_a(t)C_c(t)\\
&\qquad+C_c(t)X_5(t)+C_c(t)C_b(t)+C_c(t)^2]\\
&\quad=E\left[X_1(t)\right]E\left[X_5(t)\right]+E\left[X_1(t)\right]E\left[C_b(t)\right]\\
&\qquad+E\left[X_1(t)\right]E\left[C_c(t)\right]+E\left[C_a(t)\right]E\left[X_5(t)\right]\\
&\qquad+E\left[C_a(t)\right]E\left[C_b(t)\right]+E\left[C_a(t)\right]E\left[C_c(t)\right]\\
&\qquad+E\left[C_c(t)\right]E\left[X_5(t)\right]+E\left[C_c(t)\right]E\left[C_b(t)\right]+E\left[C_c(t)^2\right]\\
&E\left[L_{1,\mathrm{SV1}}(t)\right]E\left[L_{5,\mathrm{SV1}}(t)\right]\\
&\quad=E\left[X_1(t)+C_a(t)+C_c(t)\right]E\left[X_5(t)+C_b(t)+C_c(t)\right]\\
&\quad=\{E\left[X_1(t)\right]+E\left[C_a(t)\right]+E\left[C_c(t)\right]\}\\
&\qquad\times\{E\left[X_5(t)\right]+E\left[C_b(t)\right]+E\left[C_c(t)\right]\}\\
&\quad=E\left[X_1(t)\right]E\left[X_5(t)\right]+E\left[X_1(t)\right]E\left[C_b(t)\right]\\
&\qquad+E\left[X_1(t)\right]E\left[C_c(t)\right]+E\left[C_a(t)\right]E\left[X_5(t)\right]\\
&\qquad+E\left[C_a(t)\right]E\left[C_b(t)\right]+E\left[C_a(t)\right]E\left[C_c(t)\right]\\
&\qquad+E\left[C_c(t)\right]E\left[X_5(t)\right]+E\left[C_c(t)\right]E\left[C_b(t)\right]+E\left[C_c(t)\right]^2\\
&\mathrm{Cov}\left[L_{1,\mathrm{SV1}}(t),L_{5,\mathrm{SV1}}(t)\right]\\
&\quad=E\left[L_{1,\mathrm{SV1}}(t)L_{5,\mathrm{SV1}}(t)\right]-E\left[L_{1,\mathrm{SV1}}(t)\right]E\left[L_{5,\mathrm{SV1}}(t)\right]\\
&\quad=E\left[C_c(t)^2\right]-E\left[C_c(t)\right]^2\\
&\quad=\mathrm{Var}\left[C_c(t)\right]\\
&\quad=\lambda_{15}t.
\end{aligned}$$

Therefore, the correlation coefficient between $L_{1,\mathrm{SV1}}(t)$ and $L_{5,\mathrm{SV1}}(t)$ is obtained as

$$\begin{aligned}
\rho_{L_{1,\mathrm{SV1}},L_{5,\mathrm{SV1}}}&=\frac{\mathrm{Cov}\left[L_{1,\mathrm{SV1}}(t)\,L_{5,\mathrm{SV1}}(t)\right]}{\sqrt{\mathrm{Var}\left[L_{1,\mathrm{SV1}}(t)\right]}\sqrt{\mathrm{Var}\left[L_{5,\mathrm{SV1}}(t)\right]}}\\
&=\frac{\lambda_{15}t}{\sqrt{(\lambda_1+\lambda_{\mathrm{SV}}+\lambda_{15})t}\sqrt{(\lambda_5+\lambda_{\mathrm{SV}}+\lambda_{15})t}}\\
&=\frac{\lambda_{15}}{\sqrt{\lambda_1+\lambda_{\mathrm{SV}}+\lambda_{15}}\sqrt{\lambda_5+\lambda_{\mathrm{SV}}+\lambda_{15}}}.
\end{aligned}$$

Similarly, the correlation coefficients between other Poisson random variables are also obtained, i.e.,

$$\begin{aligned}
\rho_{L_{1,\mathrm{SV2}},L_{5,\mathrm{SV2}}}&=\frac{\lambda_{15}}{\sqrt{\lambda_1+\lambda_{\mathrm{SV}}+\lambda_{15}}\sqrt{\lambda_5+\lambda_{\mathrm{SV}}+\lambda_{15}}}\\
\rho_{L_{1,\mathrm{SV1}},L_{1,\mathrm{SV2}}}&=\frac{\lambda_{\mathrm{SV}}}{\sqrt{\lambda_1+\lambda_{\mathrm{SV}}+\lambda_{15}}\sqrt{\lambda_1+\lambda_{\mathrm{SV}}+\lambda_{15}}}\\
\rho_{L_{5,\mathrm{SV1}},L_{5,\mathrm{SV2}}}&=\frac{\lambda_{\mathrm{SV}}}{\sqrt{\lambda_5+\lambda_{\mathrm{SV}}+\lambda_{15}}\sqrt{\lambda_5+\lambda_{\mathrm{SV}}+\lambda_{15}}}.
\end{aligned}$$

The four Poisson processes $L_{1,\mathrm{SV1}}$, $L_{5,\mathrm{SV1}}$, $L_{1,\mathrm{SV2}}$, and $L_{5,\mathrm{SV2}}$ are all doubly correlated because $L_{1,\mathrm{SV1}}(t)$ is correlated to $L_{5,\mathrm{SV1}}(t)$ with a correlation coefficient $\rho_{L_{1,\mathrm{SV1}},L_{5,\mathrm{SV1}}}$, and it is also correlated to $L_{1,\mathrm{SV2}}(t)$ with a correlation coefficient $\rho_{L_{1,\mathrm{SV1}},L_{1,\mathrm{SV2}}}$, and so forth.

The Poisson process $L_{1,\mathrm{SV1}}$ models the instances of loss of lock of the L1 channel of satellite 1. The Poisson process $L_{5,\mathrm{SV1}}$ models the instances of loss of lock of the L5 channel of satellite 1. For satellite 2, $L_{1,\mathrm{SV2}}$ models the instances of loss of lock of its L1 channel, and $L_{5,\mathrm{SV2}}$ models the instances of loss of lock of its L5 channel. Therefore, $\rho_{L_{1,\mathrm{SV1}},L_{1,\mathrm{SV2}}}$ indicates a satellite-to-satellite correlation coefficient of the L1 channels, and $\rho_{L_{5,\mathrm{SV1}},L_{5,\mathrm{SV2}}}$ indicates a satellite-to-satellite correlation coefficient of the L5 channels. Similarly, $\rho_{L_{1,\mathrm{SV1}},L_{5,\mathrm{SV1}}}$ represents a frequency-to-frequency correlation coefficient of satellite 1, and $\rho_{L_{1,\mathrm{SV2}},L_{5,\mathrm{SV2}}}$ represents a frequency-to-frequency correlation coefficient of satellite 2.

Now we have a method to generate four Poisson processes $L_{1,\mathrm{SV1}}$, $L_{5,\mathrm{SV1}}$, $L_{1,\mathrm{SV2}}$, and $L_{5,\mathrm{SV2}}$ modeling both satellite-to-satellite correlation and frequency-to-frequency correlation between two satellites, from eight independent Poisson processes X_1, C_a, Y_1, X_5, C_b, Y_5, C_c, and C_d in Fig. 14, if their rates λ_1, λ_{SV}, λ_1, λ_5, λ_{SV}, λ_5, λ_{15}, and λ_{15}, respectively, can be determined.

For the simulation in Section IV-C, the fading rate of the L1 channel is obtained from the Ascension Island data as in [29] (i.e., $\lambda_1+\lambda_{\mathrm{SV}}+\lambda_{15}=1/9.71$), and the fading rate of the L5 channel, i.e., $\lambda_5+\lambda_{\mathrm{SV}}+\lambda_{15}$, is assumed the same as the fading rate of the L1 channel, i.e., $\lambda_1+\lambda_{\mathrm{SV}}+\lambda_{15}$. Let satellite-to-satellite correlation coefficients be ρ_{SV} (i.e., $\rho_{L_{1,\mathrm{SV1}},L_{1,\mathrm{SV2}}}=\rho_{L_{5,\mathrm{SV1}},L_{5,\mathrm{SV2}}}=\rho_{\mathrm{SV}}$). Then

$$\begin{aligned}
\rho_{L_{1,\mathrm{SV1}},L_{1,\mathrm{SV2}}}&=\rho_{L_{5,\mathrm{SV1}},L_{5,\mathrm{SV2}}}\\
&=\frac{\lambda_{\mathrm{SV}}}{\sqrt{\lambda_1+\lambda_{\mathrm{SV}}+\lambda_{15}}\sqrt{\lambda_1+\lambda_{\mathrm{SV}}+\lambda_{15}}}\\
&=\frac{\lambda_{\mathrm{SV}}}{\lambda_1+\lambda_{\mathrm{SV}}+\lambda_{15}}\\
&=\rho_{\mathrm{SV}}\\
\lambda_{\mathrm{SV}}&=\rho_{\mathrm{SV}}(\lambda_1+\lambda_{\mathrm{SV}}+\lambda_{15})=\frac{\rho_{\mathrm{SV}}}{9.71}.
\end{aligned}\tag{5}$$

Once a frequency-to-frequency correlation coefficient between the L1 and L5 channels is given as ρ_{15} (i.e., $\rho_{L_{1,\mathrm{SV1}},L_{5,\mathrm{SV1}}}=\rho_{L_{1,\mathrm{SV2}},L_{5,\mathrm{SV2}}}=\rho_{15}$), λ_{15} is determined as

$$\begin{aligned}
\rho_{L_{1,\mathrm{SV1}},L_{5,\mathrm{SV1}}}&=\rho_{L_{1,\mathrm{SV2}},L_{5,\mathrm{SV2}}}=\frac{\lambda_{15}}{\lambda_1+\lambda_{\mathrm{SV}}+\lambda_{15}}=\rho_{15}\\
\lambda_{15}&=\rho_{15}(\lambda_1+\lambda_{\mathrm{SV}}+\lambda_{15})=\frac{\rho_{15}}{9.71}.
\end{aligned}\tag{6}$$

Finally, λ_1 and λ_5 are also determined for the given ρ_{SV} and ρ_{15} as

$$\begin{aligned}\lambda_1+\lambda_{\mathrm{SV}}+\lambda_{15}&=\lambda_5+\lambda_{\mathrm{SV}}+\lambda_{15}=\frac{1}{9.71}\\ \lambda_1&=\lambda_5=\frac{1}{9.71}-\lambda_{\mathrm{SV}}-\lambda_{15}\\ &=\frac{1}{9.71}-\frac{\rho_{\mathrm{SV}}}{9.71}-\frac{\rho_{15}}{9.71}\\ &=\frac{1-\rho_{\mathrm{SV}}-\rho_{15}}{9.71}. \end{aligned} \tag{7}$$

Since the rates of Poisson processes λ_{SV}, λ_{15}, λ_1, and λ_5 are now determined from (5)–(7) for a given satellite-to-satellite correlation coefficient ρ_{SV} and a frequency-to-frequency correlation coefficient ρ_{15}, eight independent Poisson processes X_1, C_a, Y_1, X_5, C_b, Y_5, C_c, and C_d in Fig. 14 can be generated with corresponding rates. Therefore, doubly correlated Poisson processes $L_{1,\mathrm{SV1}}$, $L_{5,\mathrm{SV1}}$, $L_{1,\mathrm{SV2}}$, and $L_{5,\mathrm{SV2}}$ modeling the instances of L1 and L5 loss of lock of satellites 1 and 2 are obtained by combining these eight independent Poisson processes, as shown in Fig. 14.

Note that the rates of Poisson processes λ_1 and λ_5 in (7) must be positive. Hence, $\rho_{\mathrm{SV}}+\rho_{15}<1$. This means that the sum of a simulated satellite-to-satellite correlation coefficient and a frequency-to-frequency correlation coefficient must be less than 1. Therefore, if a satellite-to-satellite correlation coefficient is selected as 0.15 as in Section IV-C, only a frequency-to-frequency correlation coefficient less than 0.85 can be simulated using this method.

ACKNOWLEDGMENT

The authors appreciate the valuable comments from S. Pullen, Stanford University. The opinions discussed here are those of the authors and do not necessarily represent those of the FAA or other affiliated agencies.

REFERENCES

[1] B. W. Parkinson, "Origins, evolution, and future of satellite navigation," *J. Guid. Control Dyn.*, vol. 20, no. 1, pp. 11–25, Jan./Feb. 1997.

[2] P. Misra and P. Enge, *Global Positioning System: Signals, Measurements, and Performance*, 2nd ed. Lincoln, MA, USA: Ganga-Jamuna Press, 2006.

[3] E. D. Kaplan and C. Hegarty, *Understanding GPS: Principles and Applications*, 2nd ed. Boston, MA, USA: Artech House, 2006, ser. Artech House Mobile Communications Series.

[4] T. Walter, P. Enge, J. Blanch, and B. Pervan, "Worldwide vertical guidance of aircraft based on modernized GPS and new integrity augmentations," *Proc. IEEE*, vol. 96, no. 12, pp. 1918–1935, Dec. 2008.

[5] M. Prandini, L. Piroddi, S. Puechmorel, and S. L. Brazdilova, "Toward air traffic complexity assessment in new generation air traffic management systems," *IEEE Trans. Intell. Transp. Syst.*, vol. 12, no. 3, pp. 809–818, Sep. 2011.

[6] S. E. Campbell, "Multiscale path optimization for the reduced environmental impact of air transportation," *IEEE Trans. Intell. Transp. Syst.*, vol. 13, no. 3, pp. 1327–1337, Sep. 2012.

[7] S. Darr, W. Ricks, and K. A. Lemos, "Safer systems: A NextGen aviation safety strategic goal," *IEEE Aerosp. Electron. Syst. Mag.*, vol. 25, no. 6, pp. 9–14, Jun. 2010.

[8] C. Mario and J. Rife, "Integrity and continuity for automated surface conflict-detection monitoring," *IEEE Trans. Intell. Transp. Syst.*, vol. 13, no. 3, pp. 1179–1187, Sep. 2012.

[9] R. E. Phelts, G. Gao, G. Wong, L. Heng, T. Walter, P. Enge, S. Erker, S. Tholert, and M. Meurer, "Aviation grade: New GPS signals–chips off the Block IIF," *Inside GNSS*, vol. 5, no. 5, pp. 36–45, Jul./Aug. 2010.

[10] S. Erker, S. Tholert, M. Meurer, L. Heng, E. Phelts, G. Gao, G. Wong, T. Walter, and P. Enge, "On the air: New signals from the first GPS IIF satellite," *Inside GNSS*, vol. 5, no. 5, pp. 28–35, Jul./Aug. 2010.

[11] S. Datta-Barua, T. Walter, J. Blanch, and P. Enge, "Bounding higher-order ionosphere errors for the dual-frequency GPS user," *Radio Sci.*, vol. 43, no. 5, pp. RS5010-1–RS5010-15, Oct. 2008.

[12] Y. T. Morton, Q. Zhou, and F. van Graas, "Assessment of second-order ionosphere error in GPS range observables using Arecibo incoherent scatter radar measurements," *Radio Sci.*, vol. 44, no. 1, pp. RS1002-1–RS1002-13, Feb. 2009.

[13] S. Basu, "Equatorial scintillations—A review," *J. Atmos. Terr. Phys.*, vol. 43, no. 5/6, pp. 473–489, May/Jun. 1981.

[14] C. L. Rino, V. H. Gonzalez, and A. R. Hessing, "Coherence bandwidth loss in transionospheric radio propagation," *Radio Sci.*, vol. 16, no. 2, pp. 245–255, Mar./Apr. 1981.

[15] J. Aarons, "Global morphology of ionospheric scintillations," *Proc. IEEE*, vol. 70, no. 4, pp. 360–378, Feb. 1982.

[16] F. S. Rodrigues, E. R. de Paula, M. A. Abdu, A. C. Jardim, K. N. Iyer, P. M. Kintner, and D. L. Hysell, "Equatorial spread F irregularity characteristics over Sao Luis, Brazil, using VHF radar and GPS scintillation techniques," *Radio Sci.*, vol. 39, no. 1, pp. RS1S31-1–RS1S31-9, Feb. 2004.

[17] A. M. Smith, C. N. Mitchell, R. J. Watson, R. W. Meggs, P. M. Kintner, K. Kauristie, and F. Honary, "GPS scintillation in the high arctic associated with an auroral arc," *Space Weather*, vol. 6, no. 3, pp. S03D01-1–S03D01-7, Mar. 2008.

[18] P. M. Kintner, B. M. Ledvina, and E. R. De Paula, "GPS and ionospheric scintillations," *Space Weather*, vol. 5, no. 9, pp. S09003-1–S09003-23, Sep. 2007.

[19] Y. Beniguel and J.-P. Adam, *Effects of Scintillations in GNSS Operation*. Berlin, Germany: Springer-Verlag, 2007.

[20] T. E. Humphreys, M. L. Psiaki, J. C. Hinks, B. O'Hanlon, and P. M. Kintner, "Simulating ionosphere-induced scintillation for testing GPS receiver phase tracking loops," *IEEE J. Sel. Topics Signal Process.*, vol. 3, no. 4, pp. 707–715, Aug. 2009.

[21] T. E. Humphreys, M. L. Psiaki, B. M. Ledvina, A. P. Cerruti, and P. M. Kintner, "Data-driven testbed for evaluating GPS carrier tracking loops in ionospheric scintillation," *IEEE Trans. Aerosp. Electron. Syst.*, vol. 46, no. 4, pp. 1609–1623, Oct. 2010.

[22] T. E. Humphreys, M. L. Psiaki, and P. M. Kintner, "Modeling the effects of ionospheric scintillation on GPS carrier phase tracking," *IEEE Trans. Aerosp. Electron. Syst.*, vol. 46, no. 4, pp. 1624–1637, Oct. 2010.

[23] M. B. El-Arini, R. S. Conker, S. D. Ericson, K. W. Bean, F. Niles, K. Matsunaga, and K. Hoshinoo, "Analysis of the effects of ionospheric scintillation on GPS L2 in Japan," in *Proc. 16th Int. Tech. Meet. Satellite Div. Inst. Navig.*, 2003, pp. 314–327.

[24] J. Seo, T. Walter, T. Y. Chiou, and P. Enge, "Characteristics of deep GPS signal fading due to ionospheric scintillation for aviation receiver design," *Radio Sci.*, vol. 44, no. 1, pp. RS0A16-1–RS0A16-10, Feb. 2009.

[25] R. S. Conker, M. B. El-Arini, C. J. Hegarty, and T. Hsiao, "Modeling the effects of ionospheric scintillation on GPS/satellite-based augmentation system availability," *Radio Sci.*, vol. 38, no. 1, pp. 1001-1–1001-23, Feb. 2003.

[26] J. A. Secan, R. M. Bussey, E. J. Fremouw, and S. Basu, "High-latitude upgrade to the wideband ionospheric scintillation model," *Radio Sci.*, vol. 32, no. 4, pp. 1567–1574, Jul./Aug. 1997.

[27] A. O. Akala, P. H. Doherty, C. S. Carrano, C. E. Valladares, and K. M. Groves, "Impacts of ionospheric scintillations on GPS receivers intended for equatorial aviation applications," *Radio Sci.*, vol. 47, no. 4, pp. RS4007-1–RS4007-11, Aug. 2012.

[28] J. Seo, T. Walter, and P. Enge, "Availability impact on GPS aviation due to strong ionospheric scintillation," *IEEE Trans. Aerosp. Electron. Syst.*, vol. 47, no. 3, pp. 1963–1973, Jul. 2011.

[29] J. Seo, T. Walter, and P. Enge, "Correlation of GPS signal fades due to ionospheric scintillation for aviation applications," *Adv. Space Res.*, vol. 47, no. 10, pp. 1777–1788, May 2011.

[30] P. Enge, T. Walter, S. Pullen, C. Kee, Y. C. Chao, and Y. J. Tsai, "Wide area augmentation of the global positioning system," *Proc. IEEE*, vol. 84, no. 8, pp. 1063–1088, Aug. 1996.

[31] "Minimum operational performance standards for global positioning system/wide area augmentation system airborne equipment," Washington, DC, USA, Doc. DO-229D, 2006.

[32] H. Cabler and B. DeCleene, "LPV: New, improved WAAS instrument approach," in *Proc. 15th Int. Tech. Meet. Satellite Div. Inst. Navig.*, 2002, pp. 1013–1021.
[33] C. J. Hegarty and E. Chatre, "Evolution of the Global Navigation Satellite System (GNSS)," *Proc. IEEE*, vol. 96, no. 12, pp. 1902–1917, Dec. 2008.
[34] C. Cohenour and F. van Graas, "GPS orbit and clock error distributions," *NAVIGATION*, vol. 58, no. 1, pp. 17–28, Spring 2011.
[35] S. S. Jan, W. Chan, and T. Walter, "MATLAB algorithm availability simulation tool," *GPS Sol.*, vol. 13, no. 4, pp. 327–332, Sep. 2009.
[36] R. G. Gallager, *Discrete Stochastic Processes, ser. The Kluwer International Series in Engineering and Computer Science*. Boston, MA, USA: Kluwer, 1996.
[37] E. J. Fremouw, R. L. Leadabrand, R. C. Livingston, M. D. Cousins, C. L. Rino, B. C. Fair, and R. A. Long, "Early results from DNA Wideband satellite experiment - complex-signal scintillation," *Radio Sci.*, vol. 13, no. 1, pp. 167–187, Jan./Feb. 1978.
[38] A. J. Van Dierendonck and C. Hegarty, "The new L5 civil GPS signal," *GPS World*, vol. 11, no. 9, pp. 64–72, Sep. 2000.
[39] P. H. Doherty, C. E. Valladares, and C. Carrano, "The low-latitude ionospheric sensor network: The initial campaigns," presented at the American Geophysical Union, Spring Meeting, Toronto, ON, USA, May 24–27, 2009.
[40] S. Datta-Barua, J. Lee, S. Pullen, M. Luo, A. Ene, D. Qiu, G. Zhang, and P. Enge, "Ionospheric threat parameterization for local area global-positioning-system-based aircraft landing systems," *J. Aircraft*, vol. 47, no. 4, pp. 1141–1151, Jul./Aug. 2010.
[41] *Procedures for Air Navigation Services—Aircraft Operations, Vol. I Flight Procedures, Doc. 8168-OPS/611*, 5th ed, Int. Civil Aviation Org., Quebec, QC, Canada, 2006.
[42] S. Jung and J. Lee, "Long-term ionospheric anomaly monitoring for ground based augmentation systems," *Radio Sci.*, vol. 47, no. 4, pp. RS4006-1–RS4006-12, Aug. 2012.
[43] M. B. El-Arini, J. Secan, J. A. Klobuchar, P. H. Doherty, G. Bishop, and K. Groves, "Ionospheric effects on GPS signals in the arctic region using early GPS data from Thule, Greenland," *Radio Sci.*, vol. 44, no. 1, pp. RS0A05-1–RS0A05-14, Feb. 2009.

Jiwon Seo (M'13) received the B.S. degree in mechanical engineering (division of aerospace engineering) from Korea Advanced Institute of Science and Technology, Daejeon, Korea, and the M.S. degrees in aeronautics/astronautics and electrical engineering and the Ph.D. degree in aeronautics/astronautics from Stanford University, Stanford, CA, USA.

He was a Postdoctoral Scholar with the Global Positioning System Laboratory and the Space Environment and Satellite Systems Laboratory, Stanford University. He is currently an Assistant Professor with the School of Integrated Technology and the Yonsei Institute of Convergence Technology, Yonsei University, Incheon, Korea. His research interests include GPS-based intelligent air transportation systems; alternative positioning, navigation, and timing; and intelligent unmanned systems.

Todd Walter received the B.S. degree in physics from Rensselaer Polytechnic Institute, Troy, NY, USA, and the Ph.D. degree from Stanford University, Stanford, CA, USA, in 1993.

He is a Senior Research Engineer with the Department of Aeronautics and Astronautics, Stanford University. He has long been active in the development of the Wide Area Augmentation System and its international counterparts. His early work included some of the first operational prototyping and development of many key operational algorithms and standards in use on these systems. His research interests include the future use of the two aeronautical frequencies that are available through modernized GPS and new satellite navigation systems that are being implemented around the world.

Dr. Walter is a Fellow of the Institute of Navigation and was its President.